Plasma Science and Technology

PAPER

# Influence of target temperature on AlO emission of femtosecond laser-induced Al plasmas

To cite this article: Wei QI *et al* 2021 *Plasma Sci. Technol.* **23** 045501





Plasma Sci. Technol. **23** (2021) 045501 (8pp) https://doi.org/10.1088/2058-6272/abe52c

# Influence of target temperature on AlO emission of femtosecond laser-induced Al plasmas

**Wei QI (齐巍)[1], Qiuyun WANG (王秋云)[2,*], Junfeng SHAO (邵俊峰)[3], Anmin CHEN (陈安民)[2,*] and Mingxing JIN (金明星)[2]**

[1] Beijing Institute of Tracking and Telecommunications Technology, Beijing 100094, People's Republic of China
[2] Institute of Atomic and Molecular Physics, Jilin University, Changchun 130012, People's Republic of China
[3] State Key Laboratory of Laser Interaction With Matter & Innovation Laboratory of Electro-Optical Countermeasures Technology, Changchun Institute of Optics, Fine Mechanics and Physics, Chinese Academy of Sciences, Changchun 130033, People's Republic of China

E-mail: wqy20@mails.jlu.edu.cn and amchen@jlu.edu.cn

Received 30 December 2020, revised 7 February 2021
Accepted for publication 10 February 2021
Published 9 March 2021


**Abstract**

The influence of the target temperature on the molecular emission of femtosecond laser-induced breakdown spectroscopy (LIBS) was investigated experimentally. An Al target was ablated to produce laser-induced plasma. The Al target was uniformly heated to a maximum of 250 °C. The measured molecular emission was AlO ($\Delta\nu = 0$) from the femtosecond LIBS of the Al target. The measurements indicated that the molecular emission of AlO increased as the temperature of the Al target increased. In addition, a two-temperature model was used to simulate the evolution of the electron and lattice temperature of the Al target with different initial temperatures. The simulated results showed that the electron and lattice temperatures of Al irradiated by the femtosecond laser increased as the initial temperature of the Al target increased; also, the simulated ablated depth increased. Therefore, an increase in the initial Al target temperature resulted in an enhancement in the spectral signal of AlO from the femtosecond LIBS of Al, which was directly related to the increase in the size of the ablated crater. The study suggested that increasing the temperature of the target improves the intensity of molecular emission in femtosecond LIBS.

Keywords: laser-induced breakdown spectroscopy, femtosecond laser, sample temperature, AlO

(Some figures may appear in colour only in the online journal)

## 1. Introduction

Laser-induced breakdown spectroscopy (LIBS) is an analytical technique that has been used for many years [1–4]. It is essentially a spectroscopic technique due to the analysis of spectral signals from laser-induced plasmas. It is easy to understand the physical process of LIBS. A high-energy laser pulse is converged at a material that can be solid, liquid, or gas [5–10]. The material will be heated rapidly, vaporized, dissociated, and ionized, generating hot luminous plasma with a high temperature and a high density. When the laser pulse terminates, the plasma begins to cool in the ambient atmosphere or in a vacuum. The electrons of the atoms and ions at the excited states in the plasma transit to low states, producing a characteristic optical emission signal, which includes discrete lines, bands, and continua [11–13]. The characteristic emission is related to the natural properties of the material. Therefore, LIBS can provide qualitative and quantitative information on the material.

* Authors to whom any correspondence should be addressed.

With the development of the LIBS technique, many studies on LIBS have begun to focus on molecular emission from laser-induced plasma [14, 15]. The molecular emission technique can be used for the detection and analysis of organic materials including nitrocompounds, polymers, explosives, and biological samples [16]. Zhao *et al* demonstrated atomic and molecular spectra of laser-ablated nitromethane [17], discussing the time-resolved spectra and the formation mechanisms of CN and $C_2$. Trautner *et al* reported laser ablation of a polyethylene sample [18], they detected and simulated $C_2$ swan and CN violet and red bands. De Lucia *et al* investigated the influence of variable selection on partial least squares discriminant analysis models based on LIBS [19], showing that high nitrogen molecules and some organic materials may be identified. Samuels *et al* used LIBS to study bacterial spores, molds, and pollens [20], finding that the bacterial spores and the molds and pollens could be discriminated by LIBS. However, as compared to traditional LIBS with a nanosecond pulse laser, LIBS studies employing a femtosecond pulsed laser have shown some advantages for exploring LIBS analysis [21–28]. There are considerable physical differences between a nanosecond pulse and a femtosecond pulse for laser ablation of samples. The femtosecond laser can provide a lot of advantages in LIBS analysis, including (i) a low ablation threshold, (ii) a small heat-affected zone, (iii) a high ablation efficiency, (iv) a low continuous spectrum, and (v) a long propagation distance of a few kilometers through femtosecond laser filamentation. In addition, femtosecond laser ablation generates low-temperature plasma, which is suitable for the formation of molecules in LIBS [29, 30]. Serrano *et al* discussed the effect of pulse width on the formation of diatomic molecules by femtosecond and nanosecond laser-produced plasmas [31], demonstrating that the femtosecond laser can better reflect the material structure compared with the nanosecond laser. Kalam *et al* investigated LIBS of six high-energy materials excited by femtosecond and nanosecond lasers [32]; their results showed that molecular emission was prominent in femtosecond LIBS, while the atomic spectrum dominated nanosecond LIBS. Harilal *et al* compared molecular spectra from nanosecond, femtosecond, and filament-induced plasmas [33], finding that molecular temperatures were lower for femtosecond LIBS, and molecular species at early times for femtosecond LIBS compared with nanosecond LIBS could be observed.

The femtosecond laser presents a good advantage for molecular detection in LIBS [21–27]. In order to improve the sensitivity and practicability of femtosecond LIBS detection of molecules, it is necessary to increase the molecular emission intensity of femtosecond LIBS. From many previously published papers, several experimental techniques have been used to increase the emission intensity of LIBS [34], such as: double-pulse LIBS [35–37], spatially confined LIBS [38, 39], magnetically confined LIBS [40, 41], flame-enhanced LIBS [42, 43], nano-particle-enhanced LIBS [44], surface-enhanced LIBS [45], and discharge-assisted LIBS [46–48]. Also, increasing the sample temperature is an effective method to improve the optical signal of LIBS [49–56]. Hai *et al* explored the influence of molybdenum-tungsten target temperature on the spectra from laser-excited molybdenum-tungsten plasmas [57], finding that the spectral line emission, ablation crater, plasma temperature, and electron density increased obviously as the target was heated. Lednev *et al* studied the influence of low-alloy steel temperature on the laser-ablated process and detection sensitivity of LIBS [58], finding that increasing the surface temperature was beneficial in enhancing the spectral signal. Tavassoli *et al* investigated the influence of the aluminum sample temperature on the spectral signal of LIBS [59]; their results showed that increasing the target temperature enhanced spectral emission intensity, and thus enhanced the analysis sensitivity of the target composition. These studies discussed the relationship between atomic emission spectra and the sample temperature. It is also necessary to discuss the change in molecular emission spectra with sample temperature in femtosecond LIBS.

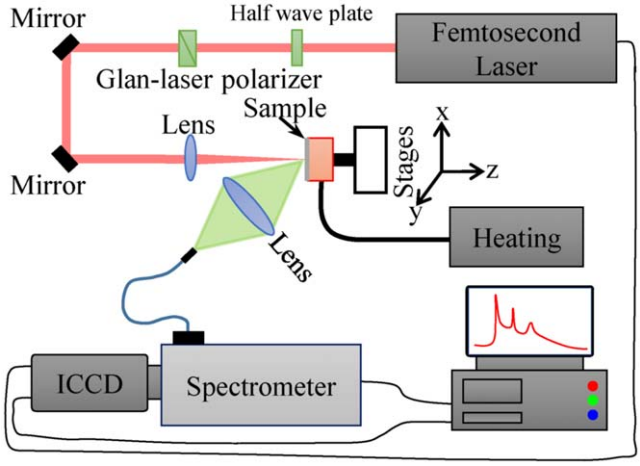


**Figure 1.** Schematic diagram of experimental setup.

This paper studies the influence of Al target temperature on the molecular emission of femtosecond laser-produced Al plasma. The emission intensity of diatomic molecular aluminum monoxide (AlO) from the Al plasma was measured at different sample temperatures. Also, we calculated the thermal dynamics of the Al target under femtosecond laser irradiation using a two-temperature equation for different Al temperatures.

## 2. Experimental setup

As can be seen in figure 1, a regeneration amplified Ti:sapphire laser (Coherent, Libra) with a wavelength of 800 nm, and a pulse duration of 50 fs, was used to ablate the aluminum plate with 99.9% purity. The laser system operated in single-shot mode was fired by sending a command ('man:trig') to the serial port (RS232) of the synchronization and delay generator (SDG). The laser energy was attenuated to an experimental value by using a combination of half-wave plate and Glan-laser prism. Next, the pulse was converged to the target surface to produce Al plasma using a focusing lens (10 cm). The diameter of the spot on the sample surface is around 200 $\mu$m. The sample was pasted on a heating table

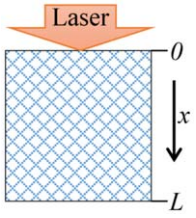


**Figure 2.** Schematic diagram of femtosecond laser irradiation of metal.

through a high thermal conductive silica gel sheet. The heating table was placed on an *X-Y-Z* stage (PT3-Z8, Thorlabs) to provide a fresh surface. The sample was uniformly heated up to a maximum of 250 °C. A thermocouple was used to monitor and feed back the sample temperature. Approximately 10 min was needed to stabilize the sample temperature during the heating process. The excited optical emission was collected by a lens with a focal length of 75 mm and a diameter of 50 mm, at an angle of 45° relative to the target surface and the laser beam direction was converged to an optical fiber, and was guided to a spectrometer with a grating of 1200 lines (PI-Acton, Princeton Instruments). The discrete optical emission of the spectrometer was detected on an ICCD (PI-MAX4, 1024I, Princeton-Instruments). Data processing is performed by a personal computer. The pulse and the ICCD were synchronized by the SDG of the femtosecond amplification system. The gain and ICCD were adjusted to 25, and the gate delay and width were set to 500 ns and 10 $\mu$s, respectively, to optimize signal intensity, eliminate continuum emission, and avoid signal saturation. Each spectrum was an average of 80 laser pulses. All of the experiments were carried out at atmospheric pressure.

## 3. Mathematical model

When a femtosecond pulse laser interacts with metal, free electrons within the metal absorb pulse energy through the inverse bremsstrahlung absorption process. The electron temperature will rise rapidly because electron thermal capacity is very small. Then, the absorbed energy is diffused deeper into the metal through the thermal diffusion of electrons, and the electron energy obtained by absorbing laser pulse energy is transferred to the lattice through the coupling between the electrons and lattice. Considering a 1D metal film (see figure 2), the temporal and spatial variations in the electron temperature ($T_e$) and the lattice temperature ($T_l$) can be expressed by a 1D two-temperature model (TTM), as follows [60–62]:

$$C_e\frac{\partial T_e}{\partial t} = \frac{\partial}{\partial x}\left(k_e\frac{\partial T_e}{\partial x}\right) - G(T_e - T_l) + S \tag{1}$$

$$C_l\frac{\partial T_l}{\partial t} = \frac{\partial}{\partial x}\left(k_l\frac{\partial T_l}{\partial x}\right) + G(T_e - T_l) \tag{2}$$

where $t$ is the delay time, $x$ is the depth, $C_e = C_{e0}T_e$ is the electron thermal capacity [63], $C_l$ is the lattice thermal capacity, $k_e = k_{e0}BT_e/(AT_e^2 + BT_l)$ is the electron heat conductivity, $k_l$ is the lattice heat conductivity, $G = G_0((AT_e + T_l)/B + 1)$ is the electron-lattice coupling coefficient, and $S$ is the laser item.

The source ($S$) can be described by the following expression [64]:

$$S = \sqrt{\frac{\beta}{\pi}}\frac{(1-R)\alpha I}{t_p}\exp\left[-\alpha x - \beta\left(\frac{t}{t_p}\right)^2\right] \tag{3}$$

where $R$ is the laser reflectivity, $\alpha$ is the laser absorption coefficient, $I$ is the laser fluence, $t_p$ is the laser pulse width, $\beta = 4\ln(2)$.

The values of $R$ and $\alpha$ for a metal are mainly due to the dielectric function $\varepsilon$ of the metal [65, 66]:

$$\varepsilon = \varepsilon_\infty - \frac{\omega_D^2}{\omega^2 + i\tau\omega} = \varepsilon_1 + i\varepsilon_2 \tag{4}$$

$\varepsilon_\infty$ is the dielectric constant, $\omega$ is the light frequency. $\omega_D = \sqrt{n_e e^2/(m_e\varepsilon_0)}$ is the plasma frequency, $n_e$, $m_e$, and $\varepsilon_0$ are the electron density, the electron mass, and the electrical permittivity of free space, respectively. $\tau$ can be expressed by [67]

$$\frac{1}{\tau} = AT_e^2 + BT_l \tag{5}$$

The real and imaginary parts are [68]:

$$\varepsilon_1 = n^2 - \kappa^2 \tag{6}$$

$$\varepsilon_2 = 2n\kappa \tag{7}$$

and

$$n = \sqrt{\frac{\varepsilon_1 + \sqrt{\varepsilon_1^2 + \varepsilon_2^2}}{2}} \tag{8}$$

$$\kappa = \sqrt{\frac{-\varepsilon_1 + \sqrt{\varepsilon_1^2 + \varepsilon_2^2}}{2}} \tag{9}$$

The reflectivity is dependent on $n$ and $\kappa$

$$R = \frac{(n-1)^2 + \kappa^2}{(n+1)^2 + \kappa^2} \tag{10}$$

The absorption coefficient is the dependence of $\kappa$

$$\alpha = \frac{2\kappa\omega}{c} \tag{11}$$

where $c$ is the speed of light in a vacuum.

Before the femtosecond laser reaches the sample, the electron and lattice systems are the target temperature ($T_0$),

$$T_e(x, 0) = T_l(x, 0) = T_0 \tag{12}$$

In the femtosecond time scale, the heat loss of the front and rear surfaces of the metal target can be neglected. The boundary conditions of equations (1) and (2) are

$$\left.\frac{\partial T_e}{\partial x}\right|_{x=0} = \left.\frac{\partial T_e}{\partial x}\right|_{x=L} = 0 \tag{13}$$

$$\left.\frac{\partial T_l}{\partial x}\right|_{x=0} = \left.\frac{\partial T_l}{\partial x}\right|_{x=L} = 0 \tag{14}$$

where $L$ is the metal thickness.

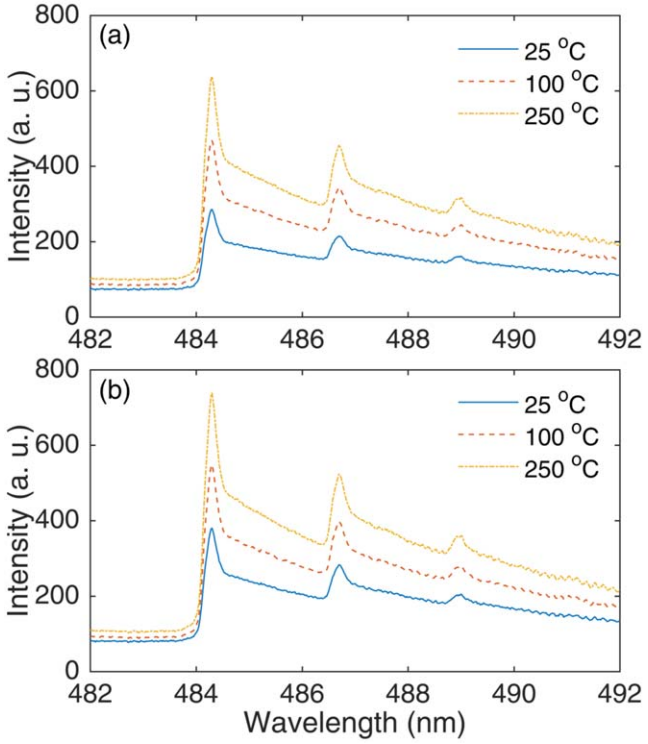


**Figure 3.** Emission spectra of AlO ($\Delta\nu = 0$) at different sample temperatures (25 °C, 100 °C and 250 °C). Laser energies are 1.4 mJ (a) and 1.9 mJ (b).

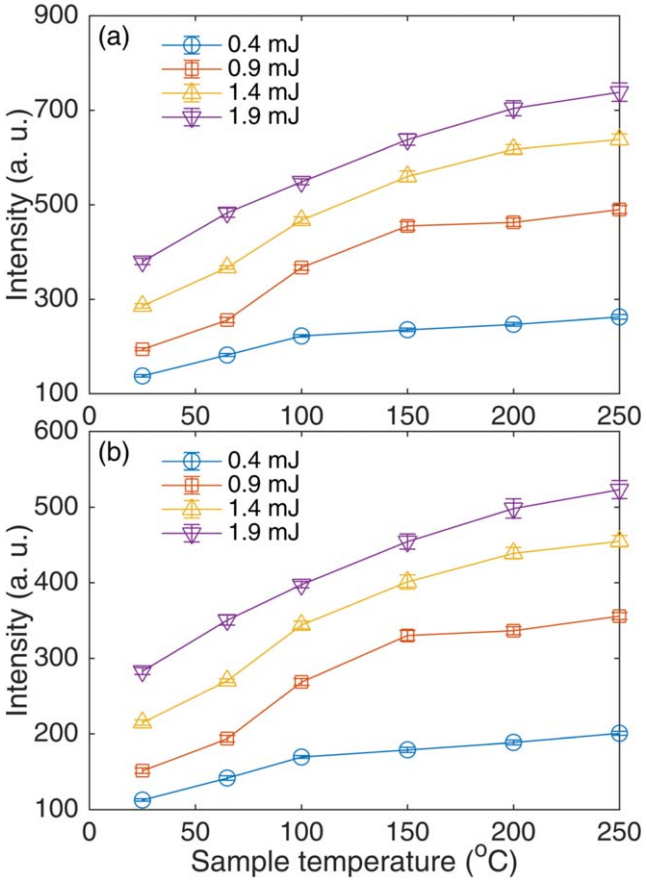


**Figure 4.** Evolution of spectral peak intensities at AlO (0–0) and (1–1) with sample temperature. Laser energies are 0.4, 0.9, 1.4 and 1.9 mJ.

## 4. Results and discussion

### *4.1. Experimental results*

In the experiment, the femtosecond pulse ablated the Al target to produce Al plasma. The molecular emission from the Al plasma was AlO diatomic radicals. The measured molecular band was the $B^2\Sigma^+$–$X^2\Sigma^+$ system with $\Delta\nu = 0$. Figure 3 presents the spectral bands of AlO ($\Delta\nu = 0$) at three sample temperatures (25 °C, 100 °C, and 250 °C) for two laser energies (1.4 and 1.9 mJ). As can be observed from the figure, when the Al target temperature increases, the spectral emission of AlO ($\Delta\nu = 0$) increases but there is no significant increase in the background emission. Moreover, the peak positions of AlO (0–0) and (1–1) are unchanged for different Al target temperatures. In our opinion, an enhancement in the signal-to-background ratio and, correspondingly, in the detection sensitivity, is possible by increasing the target temperature. Figure 4 shows the peak emission intensities of AlO (0–0) and (1–1) as functions of the Al target temperature for different laser energies. It can be seen that the emission intensities of AlO (0–0) and (1–1) increase monotonously when the Al target temperatures increase from 25 °C to 250 °C. The emission improvement can be observed at all laser energies. The results indicate that the same, or even stronger, molecular emission from laser-induced plasma, with less laser energy and higher target temperature, can be obtained.

Figure 5 shows the comparison between experimental and fitted spectra of the AlO ($\Delta\nu = 0$) molecular emission band for 0.4 and 1.9 mJ laser energies and a 25 °C sample temperature. The experimental data was fitted to get the vibrational temperature by using the existing theoretical model [69]. The fitted spectra are in agreement with the experimental spectra. The corresponding vibration temperatures are 3495 K and 3563 K for 0.4 and 1.9 mJ laser energies, respectively. Figure 6 shows the vibration temperature with the sample temperature for different laser energies. The changes in the vibration temperature with the sample temperature are similar to the changes in the AlO molecular emission with the sample temperature. The vibration temperature increases as the Al target temperature increases. Obviously, the increase in the Al target temperature enhances the interaction between the femtosecond laser and the Al target.

It is also interesting to see the influence of the sample temperature on the Al (I) line. Figure 7 presents the evolution of the Al (I) line with a sample temperature. As seen from the figure, the change in the Al (I) line is similar to the change in the AlO ($\Delta\nu = 0$) band emission as the Al target temperature increases. The result is consistent with some published results for the influence of target temperature on atomic emission line [58, 70–73]. These published results suggested that the enhancement mechanism on the emission line is due to the enhanced coupling of laser and target. To investigate the Al target ablation, the morphology of the ablation crater by

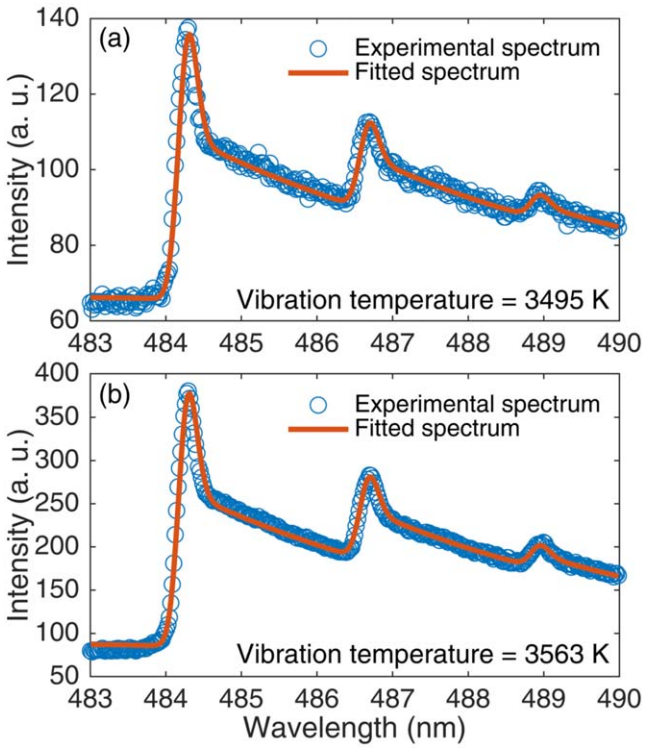


**Figure 5.** Comparison between typical experimental and fitted AlO ($\Delta\nu = 0$) emission bands for 0.4 (a) and 1.9 (b) mJ laser energies and a 25 °C sample temperature.

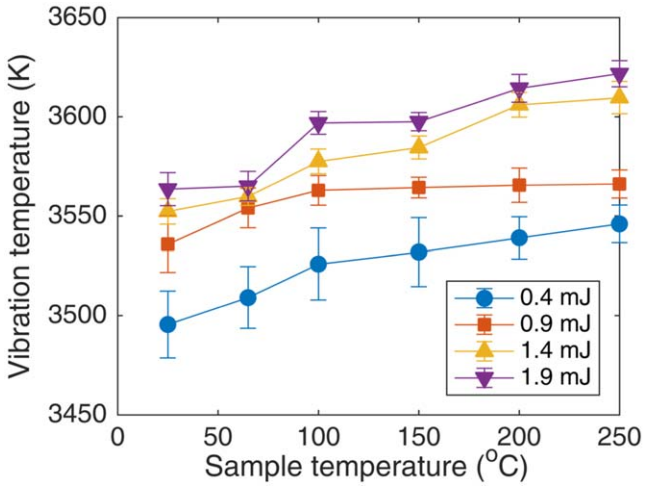


**Figure 6.** Evolution of vibration temperature with sample temperature.

femtosecond laser was measured by an optical microscope. Figure 8 presents the morphologies of the ablation craters for 0.9 and 1.9 mJ laser energies at 25 °C and 250 °C Al target temperatures. It can be observed that the ablation of the Al target surface is more obvious at high target temperature (250 °C) compared to that at low target temperature (25 °C). At the same time, compared with the melting phenomenon at 0.9 and 1.9 mJ energies, the melting phenomenon in the ablation crater at high energy is more obvious. This shows that increasing the Al target temperature enhances the absorption of femtosecond laser energy, and the energy

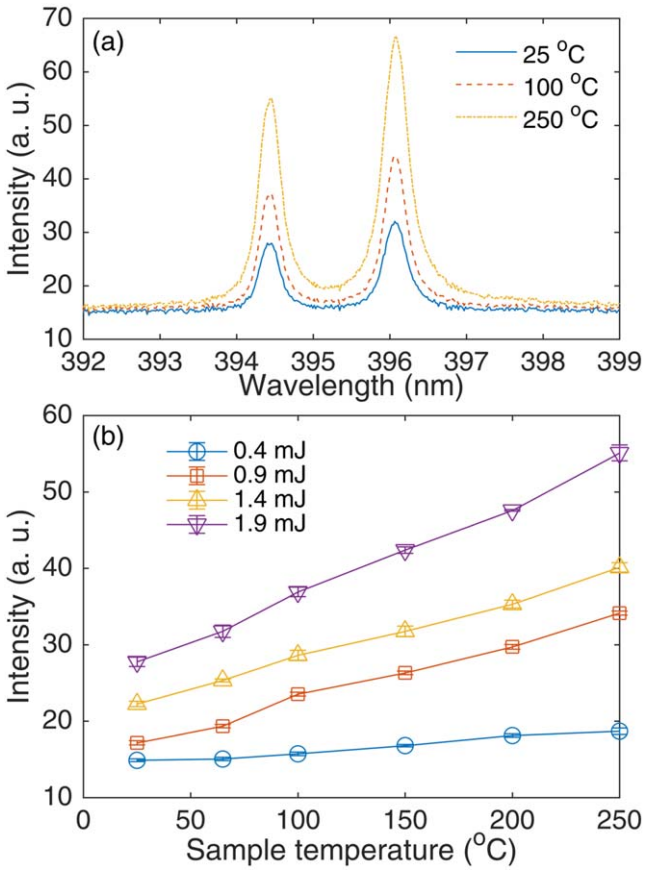


**Figure 7.** Evolution of Al (I) line with sample temperature. (a) Spectra for different sample temperatures at 1.9 mJ laser energy, (b) Al (I) 394.4 nm peak intensities as a function of sample temperature.

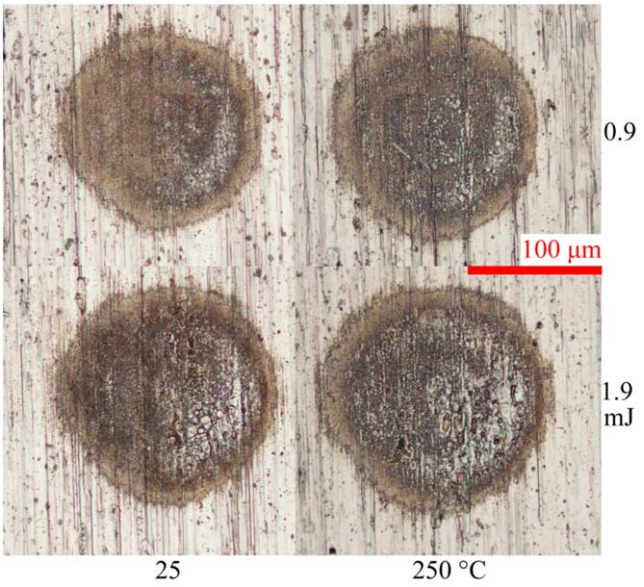


**Figure 8.** Morphologies of ablation craters by femtosecond laser for 0.9 and 1.9 mJ laser energies at 25 °C and 250 °C Al target temperatures.

needed for the Al target to melt also decreases, which makes the femtosecond laser ablation more obvious. In addition, the higher target temperature can result in a decrease in air density near the target surface, which may influence the

**Table 1.** Thermal and optical coefficients of Al used in TTM.

| Item | Value |
|---|---|
| $G_{e0}$ ($10^{17}$ J m$^{-3}$ s$^{-1}$ K$^{-1}$) | 2.45 |
| $C_{e0}$ (J m$^{-3}$ K$^{-2}$) | 134.5 |
| $k_{e0}$ (J m$^{-1}$ s$^{-1}$ K$^{-1}$) | 235 |
| $C_l$ ($10^6$ J m$^{-3}$ K$^{-2}$) | 2.42 |
| $A$ ($10^7$ s$^{-1}$ K$^{-2}$) | 0.376 |
| $B$ ($10^{11}$ s$^{-1}$ K$^{-1}$) | 3.9 |

expansion of the plasma plume; also, the change in air density will cause the change in the refractive index of air, which may lead to the change in the laser focusing condition. The two factors may influence the spectral emission intensity, and further experiments are required to be able to discuss this in detail.

### *4.2. Simulated results*

The experimental results mentioned above display an efficient enhancement in the molecular emission intensity with increasing target temperature. On the other hand, in theory, the increase in the intensity of the molecular band comes from the increase in the number of molecules. Obviously, the most direct way to increase molecular emission intensity is to increase the number of molecules. To increase the number of molecules, the ablation mass needs to be improved. At the same laser energy, increasing the target temperature enhances the interaction between laser and target. The ablation mass can be significantly increased by increasing the target temperature. In order to evaluate the effect of the Al temperature on the ablation mass, we simulated the thermal dynamics of the Al target under femtosecond laser irradiation at different target temperatures using 1D TTM, as mentioned in section 3.

For the simulation of the femtosecond pulse irradiation of Al, the laser width is 50 fs, the wavelength is 800 nm, and the simulated Al sample thickness is $L = 500$ nm. The corresponding thermal and optical coefficients are summarized in table 1 [74, 75]. Figure 9 shows the evolution of electron and lattice temperatures with the delay time for 25 °C and 150 °C sample temperatures at the sample surface. The laser fluence is 1 J cm$^{-2}$. As seen in the figure, the changes in the electron and lattice temperature are different from each other. Free electrons in the metal target absorb laser energy when the laser beam irradiates the metal, and the electron temperature rises rapidly. Next, there are two main physical processes: one is the electron heat diffusion in metal; another one is the coupling of electron and lattice, electrons transfer energy to the lattice. Due to the two physical processes, the electron temperature increases in short delay time and decreases, while the lattice temperature increases slowly, and finally the electron and lattice achieve thermal equilibrium.

In addition, the Al target temperature has a great influence on the changes in the electron and lattice temperatures. The electron temperature with the Al target temperature of 150 °C is higher than that with the Al target temperature of 25 °C. The maximum electron temperatures for 25 °C and 150 °C are 26.5 × $10^3$ K and 33.9 × $10^3$ K, respectively. The detailed changes in the lattice temperature at different sample temperatures are presented in figure 10. The surface lattice temperature becomes higher as the temperature of the Al target. The increase in the lattice temperature comes from free electrons in the metal target. Metal surface reflectivity decreases with the increase in the metal temperature. Free electrons in the Al target with higher temperature can absorb more energy from the femtosecond pulse laser. More pulse energy is transferred to the lattice, resulting in a higher lattice temperature.

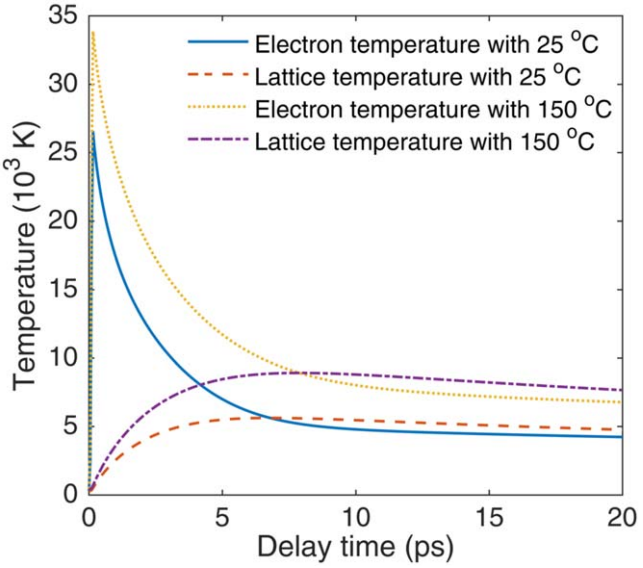


**Figure 9.** Evolution of electron and lattice temperatures with delay time for 25 °C and 150 °C sample temperatures at sample surface. Laser fluence is 1 J cm$^{-2}$.

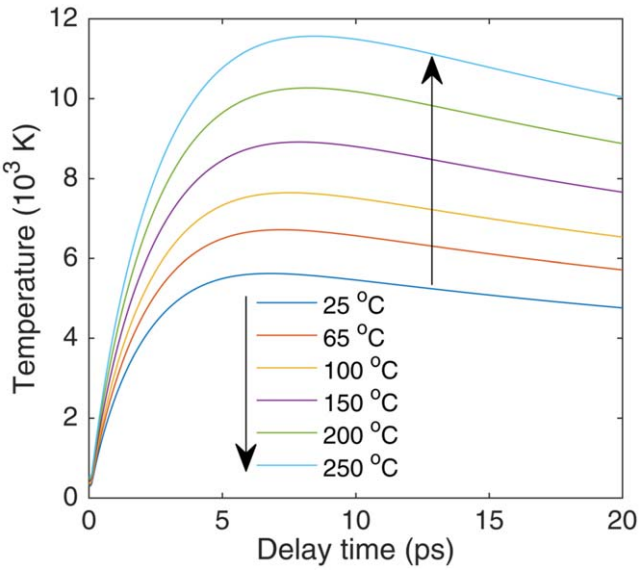


**Figure 10.** Evolution of lattice temperature with delay time for different sample temperatures at sample surface. Laser fluence is 1 J cm$^{-2}$.

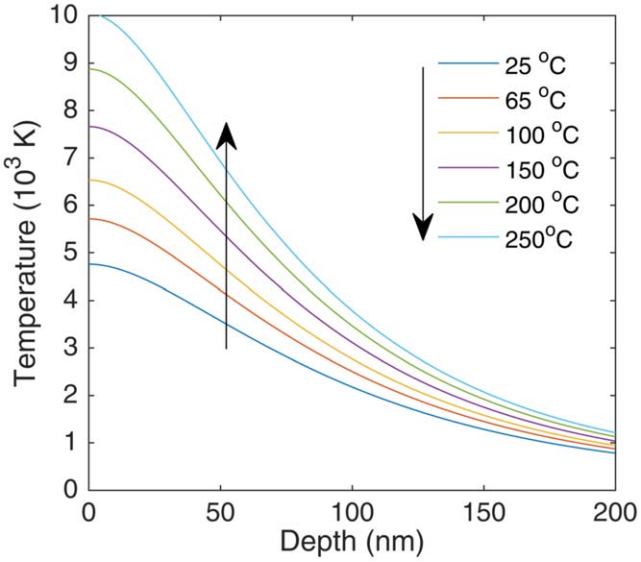


**Figure 11.** Distribution of lattice temperature with sample depth for different sample temperatures at 20 ps delay time. Laser fluence is 1 J $cm^{-2}$.

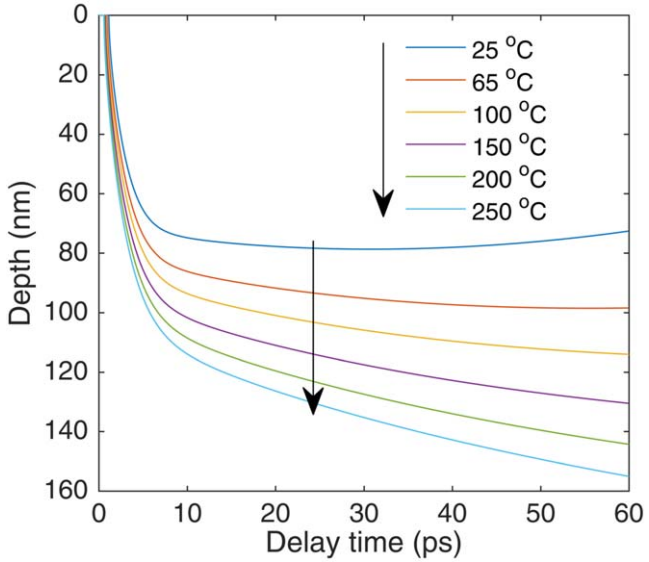


**Figure 12.** Evolution of ablation depth with delay time for different sample temperatures. Laser fluence is 1 J $cm^{-2}$.

Figure 11 presents the evolution of the lattice temperature with the sample depth for different sample temperatures at 20 ps delay time. The laser fluence is 1 J $cm^{-2}$. The initial temperature of the Al target has a great influence on the distribution of lattice temperature. When the initial target temperature increases from 25 °C to 250 °C, the surface lattice temperature rises from $4.8 \times 10^3$ K to $10.1 \times 10^3$ K; at 200 nm depth, the lattice temperature rises from $0.8 \times 10^3$ K to $1.2 \times 10^3$ K. It can be observed that the lattice temperature difference at the surface for different Al target temperatures is large, but the difference gradually decreases with the increase in the target depth, indicating that the effect of the Al sample temperature on the surface temperature is greater. When a femtosecond laser irradiates the metal surface, the electrons within the penetration depth of the target surface absorb laser energy; next, the electrons transfer the energy to a deeper target by electron thermal diffusion. More laser energy needs a longer time transfer process, so the temperature difference under higher Al temperature is bigger. Next, the ablation depth was calculated by the distribution of the lattice temperature.

Figure 12 presents the evolution of the ablation depth with the delay time for different Al target temperatures. Here, we defined that, as the lattice temperature reached the boiling point temperature of Al, the corresponding depth was evaporated and ablated. With increasing the delay time, the ablation depth gradually increases and reaches a hundred nanometers for different sample temperatures. It is also seen that the delay time of ablation becomes short from 1.1 ps to 0.5 ps, as the Al target temperature increases from 25 °C to 250 °C, and the ablation depth becomes deeper with increasing the sample temperature. That is to say, by heating the Al target, more mass Al samples can be evaporated. The simulated result may illustrate that the improvement of the molecular emission intensity is based on the enhancement in the laser ablation. The calculated results are in agreement with the experimental results (see figure 8). As discussed earlier, the evaporated depth of the sample is proportional to the molecular number within the plasma; the molecular number is proportional to the spectral emission. Thus, the improvement in the evaporated depth leads to an increase in the spectral band emission. Due to the experimental and simulated results, we can draw a conclusion that increasing the sample temperature can improve the molecular emission and the ablation depth.

## 5. Conclusion

We studied the influence of the target temperature on the AlO molecular signal from the femtosecond LIBS of Al. The emission intensity of AlO ($\Delta\nu = 0$) was measured at different target temperatures. The measured results showed that, as the Al target temperature increased, the spectral emission of AlO increased, but there was no significant increase in the background emission. In addition, the TTM was used to simulate the thermal dynamics of Al under femtosecond pulse laser irradiation for different Al target temperatures. The electron and lattice temperatures increased as the Al target temperature increased. Moreover, the ablation depth became deeper for higher Al target temperatures. A greater mass of Al material would be evaporated by raising the Al temperature. The simulated result illustrated that improvement in the molecular emission intensity is based on enhancement of the evaporated volume.

## Acknowledgments

We acknowledge the support by Scientific and Technological Research Project of the Education Department of Jilin

Province, China (No. JJKH20200937KJ), and National Natural Science Foundation of China (Nos. 11674128, 11674124, and 11974138).

## References


[1] Wang Z *et al* 2014 *Front. Phys.* **9** 419
[2] Wang Z, Dong F Z and Zhou W D 2015 *Plasma Sci. Technol.* **17** 617
[3] Wang Z Z *et al* 2016 *Front. Phys.* **11** 114213
[4] Hou Z Y *et al* 2020 *Plasma Sci. Technol.* **22** 070101
[5] Palanco S, Conesa S and Laserna J J 2004 *J. Anal. At. Spectrom.* **19** 462
[6] Wu D *et al* 2018 *Appl. Spectrosc.* **72** 225
[7] Chen A M *et al* 2015 *Phys. Plasmas* **22** 033301
[8] Yin H L *et al* 2015 *J. Anal. At. Spectrom.* **30** 922
[9] Wang Y *et al* 2016 *Phys. Plasmas* **23** 113105
[10] Chen A M *et al* 2012 *Phys. Plasmas* **19** 073302
[11] Zhang D *et al* 2020 *Optik* **202** 163511
[12] Shao J F *et al* 2020 *Optik* **207** 164448
[13] Yang L *et al* 2020 *Chin. Phys.* B **29** 065203
[14] Gaft M *et al* 2020 *Spectrochim. Acta Part B: At. Spectrosc.* **173** 105989
[15] Guo K M, Chen A M and Gao X 2020 *Optik* **208** 164067
[16] Moros J and Laserna J 2019 *Appl. Spectrosc.* **73** 963
[17] Zhao Y L *et al* 2020 *J. Hazard. Mater.* **393** 122396
[18] Trautner S *et al* 2017 *Spectrochim. Acta Part A: Mol. Biomol. Spectrosc.* **174** 331
[19] De Lucia F C and Gottfried J L 2011 *Spectrochim. Acta Part B: At. Spectrosc.* **66** 122
[20] Samuels A C *et al* 2003 *Appl. Opt.* **42** 6205
[21] Harilal S S *et al* 2014 *Appl. Phys.* A **117** 319
[22] Freeman J R *et al* 2013 *Spectrochim. Acta Part B: At. Spectrosc.* **87** 43
[23] Wang Y *et al* 2020 *Phys. Plasmas* **27** 023507
[24] Wang Q Y *et al* 2020 *Opt. Laser Technol.* **121** 105773
[25] Labutin T A *et al* 2016 *J. Anal. At. Spectrom.* **31** 90
[26] Wang X W *et al* 2017 *Phys. Plasmas* **24** 103305
[27] Yang D P *et al* 2017 *Acta Phys. Sin.* **66** 115201 (in Chinese)
[28] Shao J F *et al* 2020 *Optik* **220** 165137
[29] Wang Q Y *et al* 2020 *Opt. Laser Technol.* **122** 105862
[30] Wang Q Y *et al* 2019 *Phys. Plasmas* **26** 073302
[31] Serrano J, Moros J and Javier L 2016 *Phys. Chem. Chem. Phys.* **18** 2398
[32] Kalam S A *et al* 2017 *J. Anal. At. Spectrom.* **32** 1535
[33] Harilal S S *et al* 2016 *J. Anal. At. Spectrom.* **31** 1192
[34] Li Y C *et al* 2018 *Appl. Spectrosc. Rev.* **53** 1
[35] Shen J *et al* 2015 *Plasma Sci. Technol.* **17** 147
[36] Sun D X *et al* 2014 *Plasma Sci. Technol.* **16** 374
[37] Lin X M, Li H and Yao Q H 2015 *Plasma Sci. Technol.* **17** 953
[38] Shen X K *et al* 2007 *J. Appl. Phys.* **102** 093301
[39] Wang Y *et al* 2016 *J. Anal. At. Spectrom.* **31** 1974
[40] Lu Y *et al* 2015 *J. Anal. At. Spectrom.* **30** 2303
[41] Pandey P K and Thareja R K 2013 *Phys. Plasmas* **20** 022117
[42] Liu L *et al* 2014 *Opt. Express* **22** 7686
[43] Liu L *et al* 2015 *Opt. Express* **23** 15047
[44] De Giacomo A *et al* 2013 *Anal. Chem.* **85** 10180
[45] Aguirre M A *et al* 2013 *Spectrochim. Acta Part B: At. Spectrosc.* **79–80** 88
[46] Zhou W D *et al* 2013 *J. Anal. At. Spectrom.* **28** 702
[47] Zhou W D *et al* 2010 *Opt. Express* **18** 2573
[48] Li K X *et al* 2010 *Spectrochim. Acta Part B: At. Spectrosc.* **65** 420
[49] Eschlböck-Fuchs S *et al* 2013 *Spectrochim. Acta Part B: At. Spectrosc.* **87** 36
[50] Sanginés R, Sobral H and Alvarez-Zauco E 2012 *Spectrochim. Acta Part B: At. Spectrosc.* **68** 40
[51] Wang Y *et al* 2017 *Phys. Plasmas* **24** 013301
[52] Sanginés R, Sobral H and Alvarez-Zauco E 2012 *Appl. Phys.* B **108** 867
[53] Liu Y *et al* 2017 *Plasma Sci. Technol.* **19** 125501
[54] Shao J F *et al* 2020 *Plasma Sci. Technol.* **22** 074001
[55] Zhang D *et al* 2019 *Plasma Sci. Technol.* **21** 034009
[56] Wang Y *et al* 2019 *Plasma Sci. Technol.* **21** 034013
[57] Hai R *et al* 2019 *J. Anal. At. Spectrom.* **34** 2378
[58] Lednev V N *et al* 2019 *J. Anal. At. Spectrom.* **34** 607
[59] Tavassoli S H and Gragossian A 2009 *Opt. Laser Technol.* **41** 481
[60] Guo J *et al* 2012 *Opt. Commun.* **285** 1895
[61] Li S C *et al* 2015 *Appl. Surf. Sci.* **355** 681
[62] Li S C *et al* 2015 *Nucl. Instrum. Methods Phys. Res. Sect.* B **342** 300
[63] Kim J and Na S 2007 *Opt. Laser Technol.* **39** 1443
[64] Wang T F *et al* 2015 *Phys. Plasmas* **22** 033106
[65] Vial A and Laroche T 2008 *Appl. Phys.* B **93** 139
[66] Ren Y P, Chen J K and Zhang Y W 2011 *J. Appl. Phys.* **110** 113102
[67] Yang J, Zhao Y and Zhu X 2007 *Appl. Phys.* A **89** 571
[68] Sim H S *et al* 2010 *Mater. Trans.* **51** 1156
[69] Parigger C G *et al* 2015 *Spectrochim. Acta Part B: At. Spectrosc.* **107** 132
[70] Yang X *et al* 2019 *Acta Phys. Sin.* **68** 065201 (in Chinese)
[71] Xu W P *et al* 2019 *J. Anal. At. Spectrom.* **34** 2288
[72] Guo J *et al* 2018 *J. Anal. At. Spectrom.* **33** 2116
[73] Guo K M *et al* 2019 *AIP Adv.* **9** 065214
[74] Hu H F *et al* 2011 *Chin. Phys.* B **20** 044204
[75] Li Q *et al* 2011 *Appl. Phys.* A **105** 125